Molecular Plant Pathology

WILEY

Molecular Plant Pathology

ORIGINAL ARTICLE OPEN ACCESS

Selective Degradation of Cucumber Mosaic Virus RNA3 by Nonsense-Mediated Decay Benefits Viral Early Infection

Danqing Zhao | Md Robel Ahmed | Mengjie Tian | Mengjiao Li | Zhouhang Gu | Qiansheng Liao | Zhiyou Du

College of Life Sciences and Medicine, Zhejiang Sci-Tech University, Hangzhou, China

Correspondence: Zhiyou Du (duzy@zstu.edu.cn)

Received: 6 January 2025 | **Revised:** 14 February 2025 | **Accepted:** 14 February 2025

Funding: This work was supported by the National Natural Science Foundation of China (31870144, 32070154).

Keywords: cucumber mosaic virus | molecular interaction | nonsense-mediated decay | RNA virus | segmented genome

ABSTRACT

Nonsense-mediated mRNA decay (NMD) is a critical RNA quality control system in eukaryotes, also playing a role in defending against viral infections. However, research has primarily focused on nonsegmented viruses. To investigate the interaction between NMD and segmented RNA viruses, we used cucumber mosaic virus (CMV), which possesses a tripartite, single-stranded, positive-sense RNA genome. Agroinfiltration assays were performed to assess how CMV RNA segments, or their variants, respond to NMD. We found that CMV genomic segments (RNAs 1–3) exhibit distinct responses to NMD. Specifically, RNA3, which serves as the translation template of the movement protein (MP), is selectively degraded by NMD, unlike RNA1 and RNA2, which encode viral replicase components. This degradation is triggered by the coat protein (CP) sequence and can be mitigated by the *trans*-expression of the 1a replicase or CP. The 1a protein requires its specific interaction with the Box-B motif of RNA3 to avoid NMD. Importantly, compromising NMD reduces CMV infection during the early stages, suggesting that NMD-mediated RNA3 degradation facilitates initial viral replication. This is supported by observations that MP expression in trans negatively regulates viral RNA replication. We propose a model to illustrate the molecular interplay between NMD and CMV, emphasising the implications of genomic segmentation in NMD–virus interactions.

1 | Introduction

Positive-sense (+) RNA viruses are the most abundant class of viruses, significantly impacting eukaryotic organisms, including humans, animals and plants. To combat RNA viruses, eukaryotic hosts employ several conserved RNA regulation mechanisms, including small interfering RNA (siRNA)-mediated RNA silencing and RNA quality surveillance pathways (Lopez-Gomollon and Baulcombe 2022; Li and Wang 2019; Ding and Voinnet 2014; Ding 2010). RNA silencing plays a major role as a primary defence mechanism against viruses, particularly in plants. RNA quality surveillance pathways include nonsense-mediated decay (NMD), nonstop decay and no-go decay (Shoemaker and Green 2012). Among these pathways, NMD is the most extensively studied. It is translation-coupled and targets aberrant RNAs with premature termination codon(s) (PTCs) for degradation, minimising the production of potentially harmful truncated proteins. The core component of NMD, RNA helicase up-frameshift protein 1 (UPF1), plays a central role in recognising RNA substrates and activating NMD (Chang et al. 2007). NMD has also been characterised as a general antiviral defence mechanism since two independent studies reported NMD inhibition of viral infection in both animals and plants (Balistreri et al. 2014; Garcia et al. 2014).

During translation, if a PTC is encountered upstream of an exon junction complex (EJC), the EJC serves as a signal that triggers NMD, leading to the degradation of the faulty mRNA (Chang et al. 2007; Kashima et al. 2006). In addition to PTC, a long 3′ untranslated region (3′ UTR) can independently

activate NMD, irrespective of the presence of an EJC downstream (Kertesz et al. 2006; Hogg and Goff 2010). Numerous (+) RNA viruses possess a nonsegmented genome encoding multiple open reading frames (ORFs) that terminate separately. These RNA genomes are directly translated to produce viral proteins, typically viral replicases. During translation, ribosomes halt elongation at the termination codon of the 5′-most ORF, creating a long 3′ nontranslated sequence (3′ NTS). This long 3′ NTS renders the translating viral RNAs susceptible to NMD-mediated degradation, inhibiting viral infection (Balistreri et al. 2017; Li and Wang 2018; Popp et al. 2020; Ahmed and Du 2023). RNA viruses characterised as NMD targets typically possess a long 3′ NTS in their nonsegmented genomes. Examples include plant-infecting viruses such as potato virus X (PVX) (Garcia et al. 2014), pea enation mosaic virus 2 (PEMV2) (May et al. 2018), cucumber green mottle mosaic virus (CGMMV) (Chen et al. 2024), as well as human and animal viruses like Semliki forest virus (SFV) (Balistreri et al. 2014), Zika virus (ZIKV) (Fontaine et al. 2018), mouse hepatitis coronavirus (Wada et al. 2018) and flaviviruses such as dengue virus (DENV) and West Nile virus (WNV) (Li et al. 2019). Very recently, m^6A modification has been reported to contribute to NMD-mediated viral RNA degradation via the interaction of the m^6A reader (ETC2A) with the two NMD components, UPF3 and the suppressor with morphogenetic effect on genitalia 7 (SMG7) (He et al. 2024).

To ensure successful infection, some viruses employ strategies to escape or antagonise NMD, maintaining viral RNA integrity. A notable example is turnip mosaic virus, a representative member of the *Potyviridae* family, which evades NMD due to the absence of any internal termination codon in its genome (Garcia et al. 2014). Viruses generally use two strategies to counteract host NMD (Popp et al. 2020; Ahmed and Du 2023). The first involves *cis*-acting RNA elements, including the RNA stability element from Rous sarcoma virus (RSV) (Ge et al. 2016; Withers and Beemon 2011), the 51-nucleotide unstructured region of turnip crinkle virus (TCV) (May et al. 2018) and ribosomal decoding elements (frameshift, readthrough) from various RNA viruses (Baker and Hogg 2017; May et al. 2018; Tang et al. 2016). The second strategy involves viral proteins that inactivate NMD or assist viral RNAs in evading NMD degradation (Ahmed and Du 2023; Popp et al. 2020). The key NMD component UPF1 is often targeted for inactivation by viral proteins, such as the N-protein from coronaviruses and the coat protein (CP) from SFV and ZIKV (Emmott et al. 2013; Fontaine et al. 2018; Gordon et al. 2020; Wada et al. 2018; Contu et al. 2021). Interestingly, Du and colleagues revealed that the normal splicing of maize UPF3 pre-mRNAs is disrupted by viral nuclear inclusion protein A protease (NIa-Pro) via interaction with a splicing factor, impairing mRNA surveillance (Du et al. 2024). Additionally, other NMD factors, like the within bgcn homologue (WIBG) and the EJC-associated protein PYM1, are targeted by the core proteins or CPs of flaviviruses (Li et al. 2019; Ramage et al. 2015). Recently, PEMV2 movement protein (MP) was identified as an RNA decay inhibitor that protects both viral and host RNAs from NMD, probably by binding and shielding these RNAs (May et al. 2020).

Except for these two cases (Tran et al. 2021; Sarkar et al. 2022), studies on the interaction between NMD and viruses mainly focus on nonsegmented RNA viruses (Ahmed and Du 2023; Popp et al. 2020). In fact, RNA viruses with segmented genomes make up a considerable proportion of plant viruses. A notable example is the family *Bromoviridae*, which comprises six genera, including the two model RNA viruses brome mosaic virus (BMV) and cucumber mosaic virus (CMV). Members of the *Bromoviridae* family possess a tripartite (+) RNA genome (RNAs 1–3). RNA1 is monocistronic, encoding the replicase 1a, which localises at specific endomembranes and recruits viral and host proteins, as well as viral RNAs, to form viral replication complexes (Restrepo-Hartwig and Ahlquist 1999; Cillo et al. 2002; Baumstark and Ahlquist 2001; Noueiry and Ahlquist 2003; den Boon and Ahlquist 2010). RNA2 encodes the second replicase, 2a, which is the RNA-dependent RNA polymerase (RdRP), responsible for synthesising nascent RNAs (Poch et al. 1989; Traynor et al. 1991). Additionally, in the genera *Cucumovirus* and *Ilarvirus*, RNA2 contains a second ORF encoding the 2b protein at its 3′ proximity, partially overlapping with the 3′ portion of the 2a ORF (Ding et al. 1994; Xin et al. 1998). RNA3 is bicistronic, encoding MP and CP, which are separated by an intergenic region (IGR). The CP is translated from RNA4, a subgenomic RNA of RNA3. Both MP and CP are essential for viral movement in host plants (Canto et al. 1997), with CP also responsible for packaging viral RNAs.

To explore the potential interplay between NMD and segmented RNA viruses, here we focused on CMV, a scientifically and economically important plant pathogen (Scholthof et al. 2011; Liu et al. 2019). Our findings indicate that only RNA3, not RNA1 or RNA2, is targeted by NMD for degradation. This degradation is specifically triggered by the nucleotide sequence of the CP, while the IGR and 3′ UTR are not involved. CMV 1a or CP can compromise this degradation, possibly by spatially separating viral RNAs from translation. Importantly, we found that NMD facilitates CMV accumulation during the early stages of infection. This facilitation probably benefits from NMD-mediated RNA3 degradation, as the MP, the product of RNA3 translation, negatively regulates viral RNA replication. Our work highlights the important implication of genomic segmentation in the molecular interaction between NMD and CMV.

2 | Results

2.1 | Differential Responses of CMV RNA Variants to NMD

In plants, RNA transcripts with a 3′ UTR over 350 nt can be targeted by NMD for degradation (Kalyna et al. 2012). Given the critical role of the 3′ UTR length in activating NMD, we analysed the 3′ NTS lengths of CMV RNA segments using the model strain Fny of CMV (Fny-CMV) as a reference (Table S1). It is important to note that the 3′ NTS is equivalent to the 3′ UTR in RNA1, but this is not the case for RNA2 and RNA3. RNA3 has an exceptionally long 3′ NTS of 1257 nt, far exceeding the 350-nucleotide threshold typically associated with NMD targets in plants. However, RNA1 and RNA2 are much shorter in the length of 3′ NTS, measuring 281 and 394 nt, respectively, which are close to the 350-nucleotide threshold. Other typical viruses in the five genera within the family *Bromoviridae* display a similar pattern in their 3′ NTS size. Thus, the remarkable variation

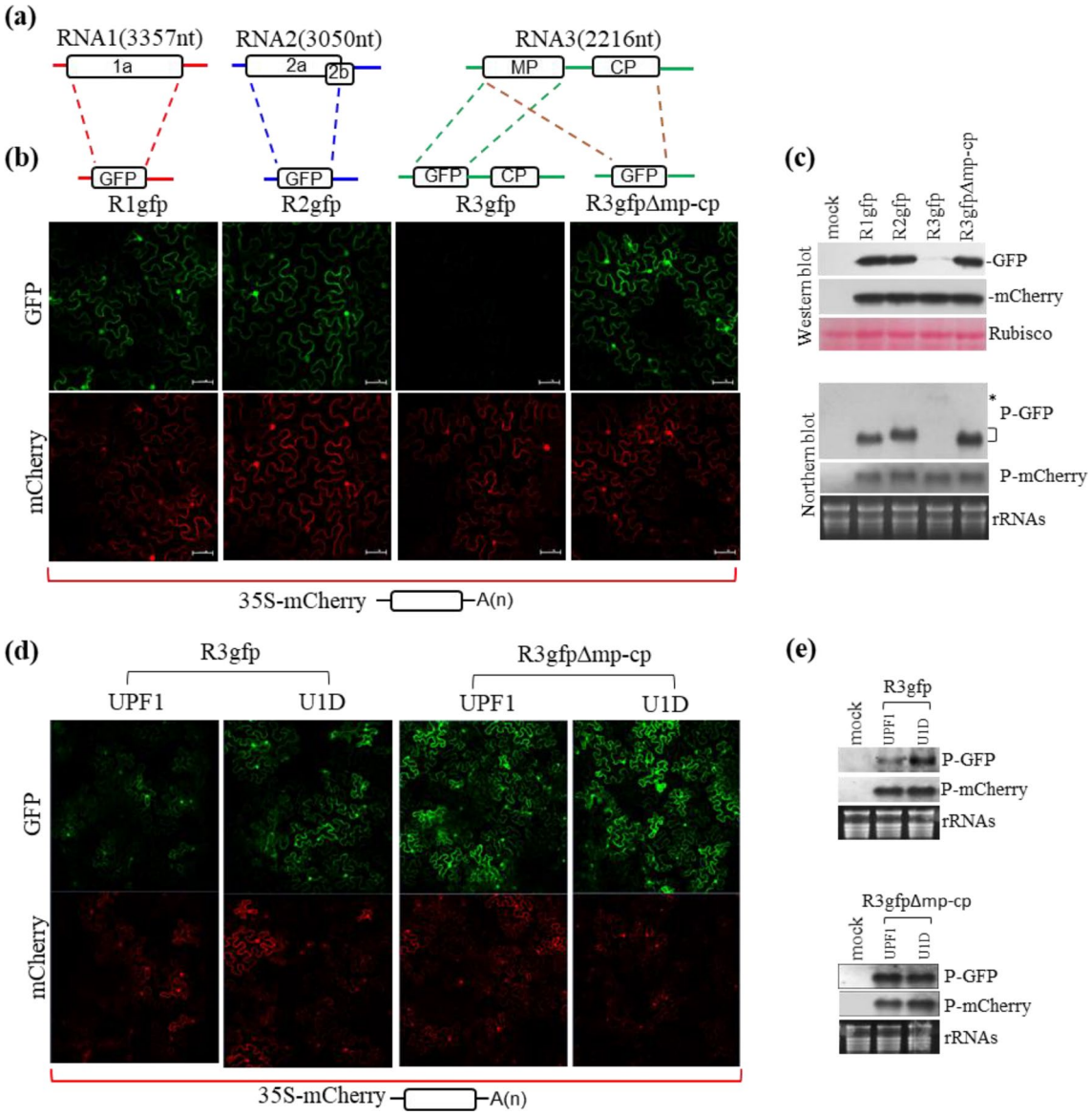

FIGURE 1 | Differential accumulation levels of GFP-expressing CMV RNA variants in Plants. (a) Schematic representation of the CMV genomic RNAs and their GFP-expressing viral RNA variants. (b, c) Transient expression of GFP-expressing viral RNA variants in *Nicotiana benthamiana* plants. Each viral RNA variant was transiently expressed along with mCherry (used as an internal control) and the silencing suppressor p19. (b) Fluorescence visualisation. At 2 days postagroinfiltration (DPAI), GFP and mCherry fluorescence was imaged in the infiltrated leaves using laser confocal microscopy with fixed laser parameters. (c) Molecular detection of these RNA transcripts by northern blot hybridization, along with their translation products by western blot hybridization, as indicated on the left. Total proteins and RNAs were extracted from the infiltrated leaves at 2 DPAI, as shown in panel (b). P-GFP and P-mCherry refer to probes specific to GFP and mCherry, respectively, and the same applies to other panels. Notably, RNA transcripts of GFP-expressing viral RNA variants were detected using a mixture of three GFP-specific probes. An asterisk indicates the position of R3gfp, while a right bracket marks the positions of the other three RNA variants. (d, e) Responses of R3gfp and R3gfpΔcp to coexpression with UPF1 or U1D. R3gfp, as well as R3gfpΔcp, was coexpressed with UPF1 or U1D, along with mCherry and p19, in the leaves of *N. benthamiana* plants. At 2 DPAI, the infiltrated leaves were collected for fluorescence visualisation (d) and RNA gel blot analysis (e), as described in the panels (b) and (c). Mock refers to the leaf samples treated with infiltration buffer.

in the 3′ NTS size suggests that CMV RNAs may have differential responses to host NMD.

To intuitively exhibit the accumulation of CMV RNAs in plants, we constructed three green fluorescence protein (GFP)-expressing variants, R1gfp, R2gfp and R3gfp, by replacing the 5′ ORF in RNA1, RNA2 and RNA3 with enhanced GFP (Figure 1a). We then performed agroinfiltration assays in *Nicotiana benthamiana* to assess these RNAs, alongside the NMD-resistant internal control 35S-mCherry in the presence of the RNA silencing suppressor p19. At 2 days postagroinfiltration (DPAI), leaves expressing R1gfp or R2gfp showed similarly strong green fluorescence, while leaves expressing R3gfp exhibited barely detectable green fluorescence (Figure 1b). Interestingly, another RNA3 variant, R3gfpΔmp-cp, in which the sequence spanning from MP to CP in RNA3 was replaced with enhanced GFP, produced strong green fluorescence equivalent to that of R1gfp or R2gfp (Figure 1b). The differences in

fluorescence intensity between R3gfp and the other RNAs were further confirmed by western blotting for GFP and northern blotting for these RNA transcripts (Figure 1c). The internal control 35S-mCherry showed consistent red fluorescence intensity and expression levels across all samples (Figure 1b,c). These findings strongly suggest that R3gfp transcripts were unstable in plants.

To determine whether the low level of R3gfp transcripts was caused by NMD, we tested the responses of R3gfp and R3gfpΔmp-cp to transiently coexpressed *Arabidopsis* UPF1 or its dominant-negative mutant U1D (Kertesz et al. 2006). Coexpression of U1D significantly enhanced green fluorescence from R3gfp compared to UPF1 expression (Figure 1d), corresponding with an increased RNA accumulation analysed by northern blotting (Figure 1e). However, no discernible difference was observed in fluorescence intensity or RNA levels of R3gfpΔmp-cp when coexpressed with U1D or UPF1 (Figure 1d,e). As expected, the expression level of the internal control 35S-mCherry remained consistent under both UPF1 and U1D conditions for each RNA variant (Figure 1d,e). These data demonstrate that, unlike R3gfpΔmp-cp, R3gfp was sensitive to NMD, leading to its instability in plants.

2.2 | RNA1 and RNA2, but Not RNA3, Are Resistant to NMD

The results shown above led us to hypothesise that RNA1 and RNA2 are resistant to NMD, whereas RNA3 is not. To test this hypothesis, we transiently coexpressed each of these three RNAs with either UPF1 or U1D via agroinfiltration in *N. benthamiana*. As expected, coexpression of U1D had no discernible effect on the RNA levels of RNA1 or RNA2 (Figure 2a,b), while it significantly increased the RNA3 level by 137% (Figure 2c) when compared to coexpression of UPF1. These results provide solid evidence that RNA1 and RNA2, but not RNA3, are resistant to NMD.

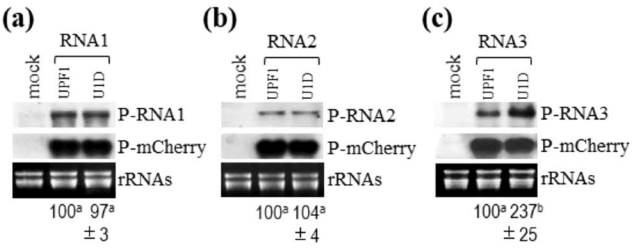

FIGURE 2 | RNA3 is sensitive to nonsense-mediated mRNA decay (NMD), while RNA1 and RNA2 are not. (a–c) Responses of RNAs 1–3 to coexpression with UPF1 or U1D. Each RNA was coexpressed with UPF1 or U1D, along with mCherry and p19, in the leaves of *Nicotiana benthamiana* plants via agroinfiltration. At 2 days postagroinfiltration (DPAI), the infiltrated leaves were collected for RNA extract and gel blotting analyses of RNA1 (a), RNA2 (b) or RNA3 (c) using RNA-specific probes. P-RNA1, P-RNA2 and P-RNA3 refer to probes specific to RNA1, RNA2 and RNA3, respectively. Mock refers to the leaf samples treated with infiltration buffer. Relative accumulation levels were calculated from three independent biological experiments with standard errors. Paired *t* test was used to analyse statistical significance. Different superscript letters indicate statistical difference at $p < 0.05$.

We were curious whether RNA1 and RNA2 also become sensitive to NMD if a PTC is introduced into their coding sequence, generating a long 3′ NTS. Interestingly, introducing an artificial PTC into RNA1 at position 1100 nt or 2096 nt (Figure S1a) resulted in the instability of both RNA1 mutants ($R1_{PTC1100}$, $R1_{PTC2096}$), as evidenced by their undetectable levels (Figure S1b). Similar influences were observed when an artificial PTC was introduced into RNA2 at position 1095 nt or 1884 nt (Figure S1a,b). As expected, coexpression with U1D increased the accumulation levels of both RNA1 mutants (Figure S1c), as well as both RNA2 mutants (Figure S1d). These results suggest that the relatively short 3′ NTS is not effective in inducing NMD against RNA1 and RNA2.

2.3 | The CP Sequence Triggers NMD

The finding that RNA3 is targeted by NMD led us to investigate which sequence within RNA3 is responsible for activating NMD. To this end, we tested the accumulation levels of R3gfp and its derivatives with deletion of the IGR (R3gfpΔigr), the 5′ half (R3gfpΔ$cp_{1\text{-}329}$) or the 3′ half (R3gfpΔ$cp_{330\text{-}657}$) of the CP (Figure 3a). The CP was divided into two halves to ensure that these deletion mutants retained similarly long 3′ NTSs, ranging from 929 to 960 nt (Figure 3a). Northern blot showed that, compared to R3gfp, R3gfpΔigr exhibited a similarly low level, while deletion of the 5′ half (R3gfpΔ$cp_{1\text{-}329}$) or the 3′ half (R3gfpΔ$cp_{330\text{-}657}$) of the CP increased the RNA level by 252% and 175%, respectively (Figure 3b). These findings were consistent with the western blot analysis of GFP (Figure 3b). Thus, both halves of the CP sequence can trigger NMD, whereas the IGR does not. Coexpression of U1D increased the RNA level of R3gfpΔ$cp_{1\text{-}329}$ by 212%, accompanied by a 133% increase in GFP protein when compared to coexpression with UPF1 (Figure 3c). Similarly, R3gfpΔ$cp_{330\text{-}657}$ increased substantially in the presence of U1D (Figure 3d). This indicates that both halves of the CP sequence independently trigger NMD. Deleting the entire CP sequence from R3gfp rendered the mutant R3gfpΔcp completely resistant to NMD, as no difference in RNA transcript levels or translation products was observed between UPF1 and U1D (Figure 3e). Additionally, when the CP sequence was fused with GFP in R3gfp → cp by removing the GFP termination codon in R3gfpΔigr (Figure 3a), the RNA and GFP-CP fusion protein levels increased greatly compared to R3gfpΔigr (Figure 3f). Furthermore, R3gfp → cp transcripts turned out to be insensitive to NMD, despite the presence of the CP sequence (Figure 3g). These data strongly suggest that the untranslated CP sequence, rather than the IGR or 3′ UTR, triggers NMD, leading to the accelerated degradation of R3gfp in plants.

Previously, May and colleagues determined that TCV 3′ UTR (250 nt in length) has the ability to inhibit NMD induced by a 747 nt-long 3′ UTR when it is posited upstream of this long 3′ UTR in a reporter RNA (May et al. 2018). We were curious whether the TCV 3′ UTR is effective as well in the inhibition of CMV CP-induced NMD. To this end, we replaced the IGR with TCV 3′ UTR in the reporter R3gfp and tested this mutant (R3gfp-$3U_{TCV}$) along with R3gfp via agroinfiltration assays where 35S-mCherry and p19 were coexpressed. Unexpectedly, the replacement did not increase the accumulation levels of the R3gfp transcripts and its translation products (Figure S2),

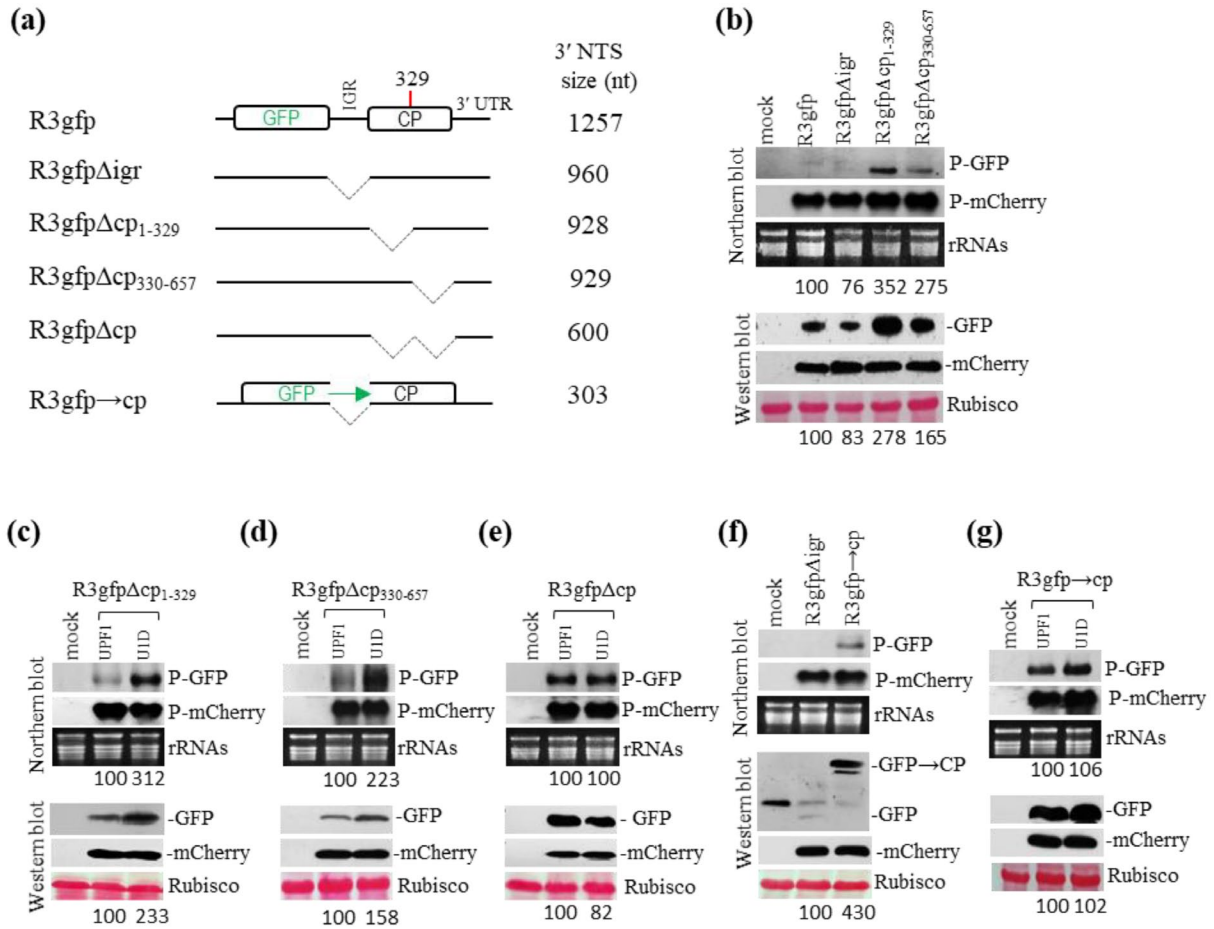

FIGURE 3 | Determination of viral RNA sequences responsible for the activation of nonsense-mediated mRNA decay (NMD). (a) Schematic diagrams of R3gfp and its derivatives with deletions of the intergenic region (IGR), the 5′ half (1–329), 3′ half (330–657) or the entire coat protein (CP) sequence. R3gfp→cp was generated by deleting the termination codon of GFP and the IGR, allowing the CP to be translated together with GFP, as indicated by a green arrow. The size of 3′ nontranslated sequence (3′ NTS) of these RNAs are shown on the right. (b) Relative accumulation levels of R3gfp and its derivatives in plants. R3gfp and its derivatives were individually expressed, along with mCherry and p19, in the leaves of *Nicotiana benthamiana* plants via agroinfiltration. P-GFP and P-mCherry refer to probes specific to GFP and mCherry, respectively, and the same applies to other panels. (c–e) Responses of the CP deletion mutants to UPF1 or U1D in plants. The CP deletion mutants, including R3gfpΔcp$_{1\text{-}329}$ (c), R3gfpΔcp$_{330\text{-}657}$ (d) and R3gfpΔcp (e), were separately coexpressed with UPF1 or U1D, along with mCherry and p19, in the leaves of *N. benthamiana*. (f) Translation of the CP sequence as a fusion protein with GFP increased RNA accumulation. R3gfpΔigr and R3gfp→cp were separately coexpressed with both mCherry and p19 in the leaves of *N. benthamiana* via agroinfiltration. For all these experiments shown in panels (b) to (g), at 2 days postagroinfiltration, the infiltrated leaves were collected for total RNA and protein extraction, which were subjected to northern blot and western blot analyses, respectively. Relative accumulation levels of RNA transcripts or GFP protein from RNA3gfp or its derivatives are shown below. Mock is the leaf samples treated with infiltration buffer.

suggesting that TCV 3′ UTR could not overcome the CP-induced NMD.

2.4 | RNA Features of the 3′ NTS From CMV RNA3

Several studies have reported that a high GC content (> 58%) in the 3′ UTRs of UPF1 targets is a key feature for inducing UPF1-mediated RNA decay (Imamachi et al. 2017; May et al. 2018). However, we found that none of the IGR, 3′ UTR, CP, or its two halves has an overall high GC content (Figure 4a). Specifically, the IGR has a notably low GC content (40.74%). Unlike the IGR, the 3′ UTR, which also does not trigger NMD, has a relatively high GC content (52.12%). Similarly, the 3′ UTRs of RNA1 and RNA2 have nearly identical GC content to that of RNA3 (Figure S3a), despite sequence variations at the beginning of their 5′ ends (Figure S3b). The complete CP and its two halves also have a regular GC content around 50%, which is even lower than that of the 3′ UTR. Therefore, we did not find a strong relationship between the overall GC content of these sequences and their different ability to induce NMD.

Local GC-rich motifs in the 3′ UTR of NMD targets are required for UPF1-mediated RNA decay (Imamachi et al. 2017), which prompted us to search for local GC- or AU-rich motifs in the 3′ NTS by scanning the 3′ NTS sequence in 50-nt windows, stepped by one nucleotide (Figure 4b). We identified two GC-rich local regions within the CP, which are separately located at the 5′ vicinities of both CP halves. The GC content in these regions reaches 71.6% and 62.0%, respectively. In

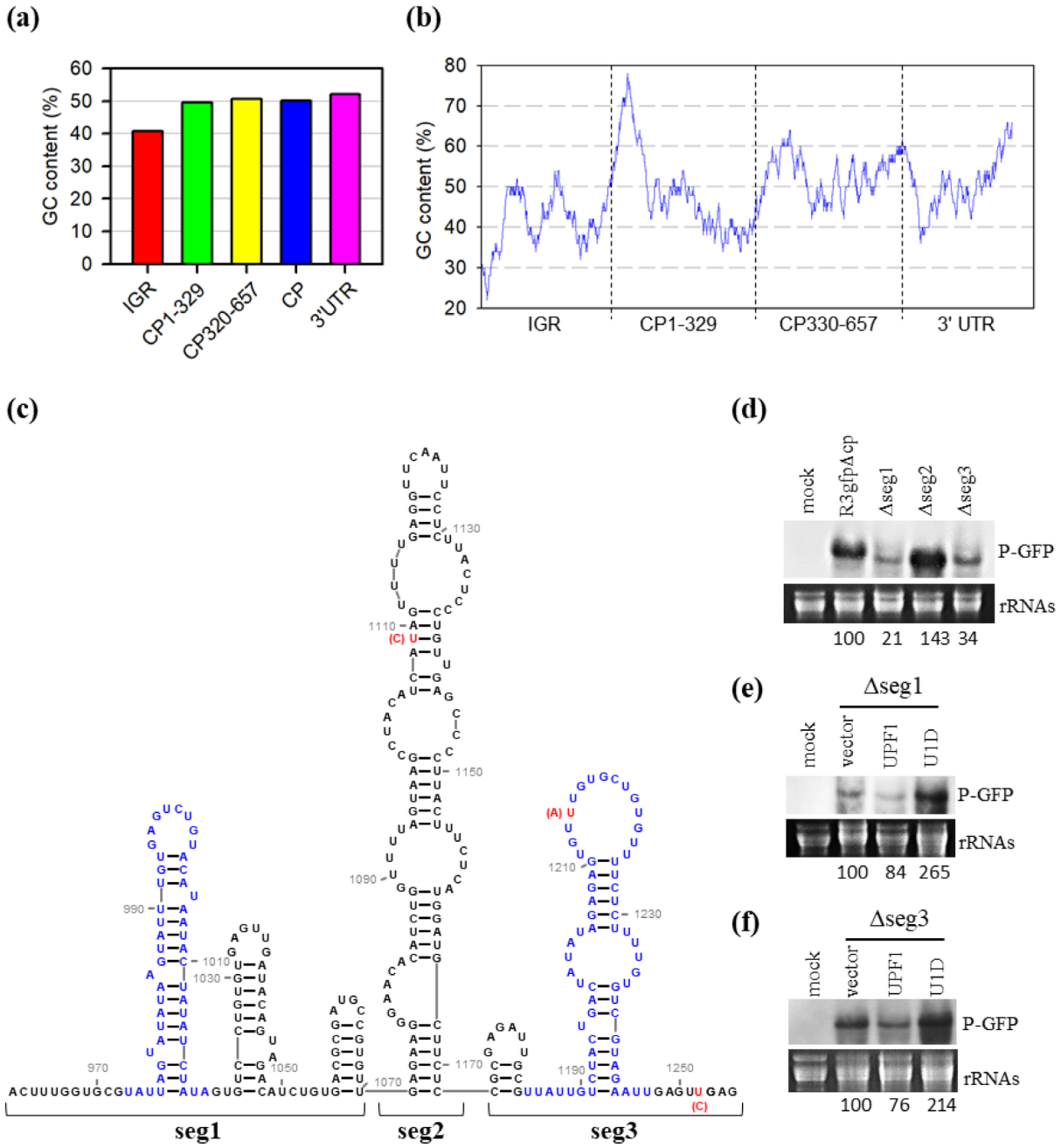

FIGURE 4 | Nonsense-mediated mRNA decay (NMD)-associated sequence features of the 3′ nontranslated sequence (NTS). (a) GC content analysis of the intergenic region (IGR), the 5′ half, 3′ half and the entire coat protein (CP) sequence, and 3′ untranslated region (UTR). (b) Scanning GC content of the 3′ NTS in a 50-nt window, stepped by one base. (c) Predicted RNA structure of the IGR. The structure was inferred from the predicted IGR of Bn57-CMV (Watters et al. 2018). Nucleotides coloured red indicate these three nucleotide differences between the IGRs of Fny-CMV and Bn57-CMV. Nucleotides coloured blue represent the AU-rich sequences. The IGR is divided into three segments based on its structure, labelled as seg1, seg2 and seg3. (d) Effect of deleting seg1, seg2 or seg3 on the accumulation of R3gfpΔcp in plants. R3gfpΔcp and these deletion mutants were individually expressed, along with p19, in the leaves of *Nicotiana benthamiana* plants via agroinfiltration. At 2 days postagroinfiltration (DPAI), infiltrated leaves were collected for RNA extraction, followed by northern blot hybridization with GFP-specific probes (P-GFP). (e, f) Responses of the Δseg1 and Δseg3 mutants to the expression of UPF1 or U1D. Δseg1 and Δseg3 were separately coexpressed with p19, along with the vector (pCambia3101), UPF1, or U1D in the leaves of *N. benthamiana* plants. At 2 DPAI, accumulation levels of Δseg1 and Δseg3 were detected through northern blot analyses with a GFP-specific probe. The relative accumulation levels are shown below. Mock refers to the leaf samples treated with infiltration buffer.

contrast, the IGR lacks GC-rich regions and instead has two AU-rich local regions located at its 5′ (down to 22.0%) and 3′ (down to 32.0%) ends. The 3′ UTR has one region with a low GC content (36.0%) at its 5′ end and another region with a high GC content (66.0%) at its 3′ end. These regions with unusual GC content might represent RNA features that determine their response to NMD.

Although the IGR cannot confer resistance against NMD in the full-length RNA3 and R3gfp (Figures 2c and 3b), it is resistant

to NMD when the CP is deleted in R3gfp (Figure 3e). We were curious whether this NMD-resistance property of the IGR is rendered by a specific sequence in the absence of the CP. To this end, we divided the IGR into three segments (seg1–3) based on its predicted RNA structure (Figure 4c). The IGR structure was inferred from that of the IGR of Bn57-CMV, which was chemically probed in plant cell lysates (Watters et al. 2018). The IGR sequences of Fny-CMV and Bn57-CMV differ by only three nucleotides, marked in red in Figure 4c. Segment 2 (seg2) folds into an extended hairpin structure that is highly conserved in certain members of the family *Bromoviridae* (Baumstark and Ahlquist 2001). Seg1 and seg3, located upstream and downstream of seg2, contain AU-rich regions, indicated in blue in Figure 4c. Agroinfiltration assays were conducted to examine the accumulation level of R3gfpΔcp and its variants with deletions of seg1, seg2 or seg3, coexpressed with p19 in the leaves of *N. benthamiana*. Deletion of seg2 (Δseg2) slightly increased RNA levels, while deletion of either seg1 (Δseg1) or seg3 (Δseg3) dramatically reduced RNA levels to 21% or 34% of R3gfpΔcp, respectively (Figure 4d). Coexpression of UPF1 slightly reduced the RNA levels of Δseg1 and Δseg3 when compared to the vector control (Figure 4e,f). In contrast, coexpressing U1D substantially increased the RNA levels of Δseg1 and Δseg3 by 165% or 114%, respectively (Figure 4e,f). These results indicate that Δseg1 and Δseg3 are highly sensitive to NMD, which is distinct from the insensitivity of R3gfpΔcp to NMD (Figure 3e). Taken together, when the CP is absent, seg1 and seg3 confer the IGR resistance against NMD, which might be due to their AU-rich feature.

2.5 | CMV 1a and CP Proteins Stabilise NMD-Sensitive R3gfp in Plants

Next, we sought to explore whether any viral protein(s) could inhibit NMD-mediated RNA3 turnover. Agroinfiltration assays were conducted in the leaves of *N. benthamiana* plants to transiently express individual CMV proteins along with R3gfp, mCherry and p19. RNA gel blotting analysis showed that the expression of either the 1a or CP protein significantly increased R3gfp transcript levels by 183% and 117%, respectively, compared to the vector control (Figure 5). Surprisingly, the level of GFP, the translation product of R3gfp, remained nearly unchanged in the presence of the 1a or CP (Figure 5). Three other viral proteins (2a, 2b, MP) were unable to enhance the accumulation level of R3gfp transcripts (Figure 5). As usual, 35S-mCherry showed consistent levels of RNA transcripts and translation products across all treatments. These distinct effects of CMV 1a and CP on RNA and protein levels suggest that these two viral proteins may sequester R3gfp transcripts from translation, preventing the RNA from entering the NMD pathway, resulting in the increase of RNA accumulation, but not translation products.

2.6 | CMV 1a Protein Stabilises R3gfp via Its Recruitment Elements

BMV 1a protein is well known for stabilising viral RNA3 by recruiting it into viral replication compartments, which depend on the amphipathic helix A domain in the 1a protein and the Box-B motif in the IGR of RNA3 (Sullivan and Ahlquist 1999;

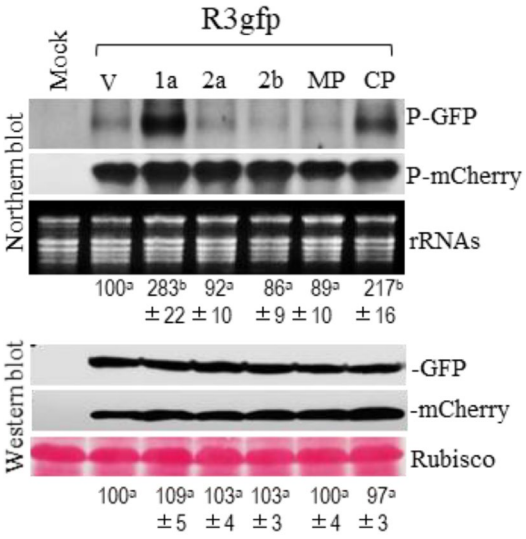

FIGURE 5 | *Trans*-expression of CMV 1a or coat protein (CP) enhances the accumulation level of R3gfp in plants. R3gfp was coexpressed with a control vector (pBI121) or one of viral proteins, together with mCherry and p19 in the leaves of *Nicotiana benthamiana* via agroinfiltration. At 2 days postagroinfiltration, the infiltrated leaves were collected for total protein and RNA extraction, followed by western blotting and northern blotting, respectively. P-GFP and P-mCherry refer to probes specific to GFP and mCherry, respectively. Mock refers to the leaf samples treated with infiltration buffer only. The relative accumulation levels of R3gfp RNA transcripts and GFP protein were calculated from three independent biological experiments with standard errors. One-way ANOVA was used to assess significant difference with $p < 0.05$, indicated by different superscript letters.

Liu et al. 2009). Inspired by these findings, we performed sequence alignment to search for regions in CMV 1a protein homologous to the helix A domain (Figure 6a). Although the residue compositions of the BMV and CMV helix A domains differ markedly, they were predicted to form nearly identical alpha helical structures (Figure S4a). Additionally, the CMV helix A domain contains a hydrophobic face with residues I426–L427–L437 (Figure S4b), similar to the L396–L400–L407 residues on the BMV helix A domain (Liu et al. 2009). Deletion of the helix A domain in the CMV 1a protein (1aΔ18H) resulted in a loss of biological activity in replicating CMV RNA3 when coexpressed with the CMV 2a protein (Figure S5). This is consistent with previous findings for BMV 1a mutant lacking the helix A domain (Liu et al. 2009).

We next investigated the impact of the wild-type CMV 1a or its mutant (1aΔ18H) on the accumulation of R3gfp RNA transcripts via agroinfiltration assays. Northern blot analyses revealed that the deletion of the helix A domain reduced R3gfp RNA levels by 82% (1a vs. 1aΔ18H) while increasing GFP protein levels by 64% (Figure 6b). Similarly, in the presence of the wild-type 1a, the deletion of the Box-B motif in R3gfp (R3gfpΔBox-B) dramatically reduced RNA levels but increased protein levels (Figure 6c,d). When coexpressed with U1D, both RNA and protein levels of R3gfpΔBox-B increased compared to the coexpression of UPF1 (Figure 6e). Taken together, these results strongly suggest that CMV 1a protein stabilises R3gfp by preventing this RNA from entering the translation process, thereby circumventing NMD-mediated degradation.

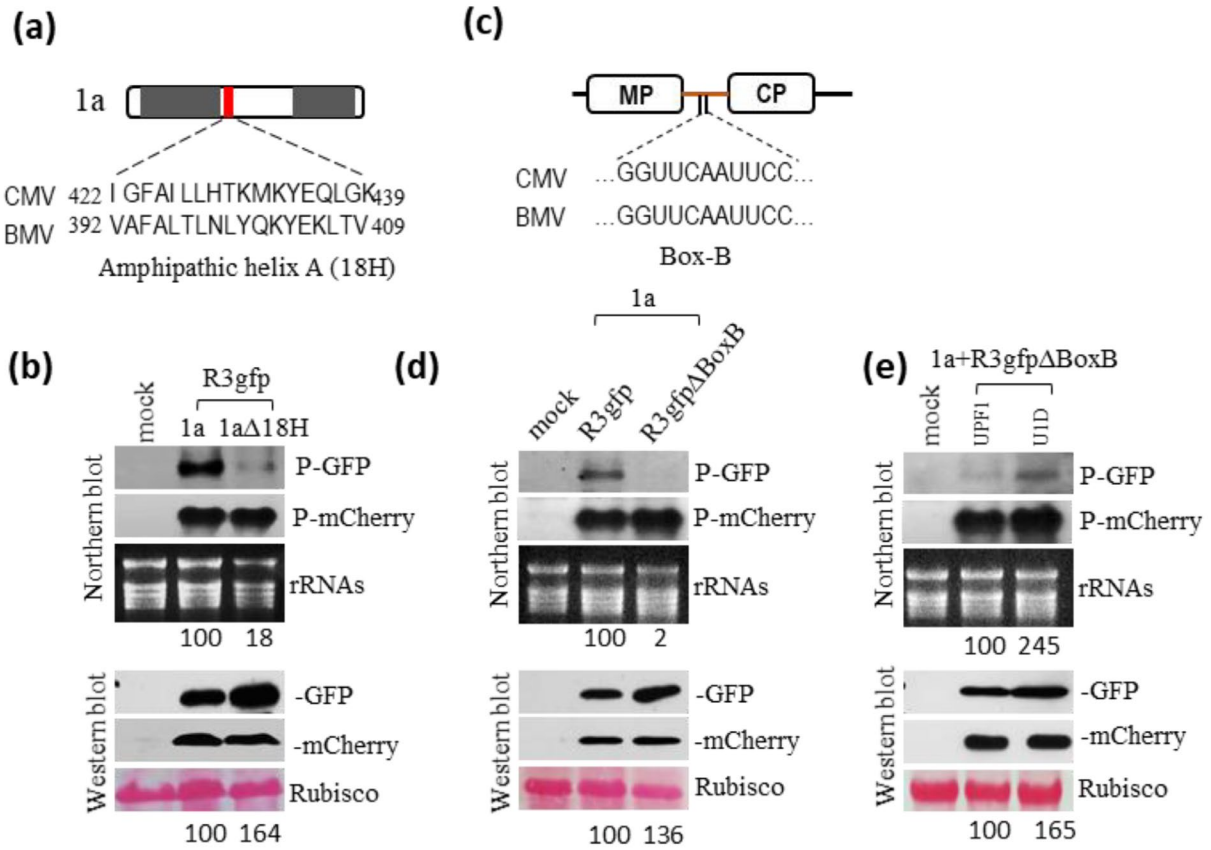

FIGURE 6 | Recruitment-associated elements are necessary for CMV 1a protein to enhance the accumulation level of R3gfp in plants. (a) The predicted amphipathic helix A in CMV 1a protein, aligned with the corresponding helix in the 1a protein of brome mosaic virus (BMV). (b) The amphipathic helix A is required for CMV 1a to increase the accumulation level of R3gfp in plants. R3gfp was coexpressed with either the wild-type 1a or its mutant lacking the amphipathic helix A (Δ18H), along with mCherry and p19 in *Nicotiana benthamiana* leaves via agroinfiltration. At 2 days postagroinfiltration, infiltrated leaves were collected for total RNA and protein extraction, followed by northern and western blotting, respectively. P-GFP and P-mCherry refer to probes specific to GFP and mCherry, respectively, and the same applies to other panels. The relative accumulation levels of R3gfp RNA transcripts and GFP protein are shown below. (c) Schematic representation of the Box-B motif in RNA3s of CMV and BMV. (d) CMV 1a protein could not stabilise the R3gfp mutant lacking the Box-B motif in plants. CMV 1a was coexpressed with either R3gfp or R3gfpΔBoxB, along with mCherry and p19, in the leaves of *N. benthamiana* via agroinfiltration. RNA and protein detection and relative quantification were performed as in (b). (e) R3gfpΔBoxB retained sensitive to nonsense-mediated mRNA decay (NMD), even in the presence of CMV 1a protein. R3gfpΔBoxB was coexpressed with UPF1 or U1D, along with CMV 1a, mCherry and p19 in *N. benthamiana* leaves. Molecular detection and quantification of target RNAs and proteins were conducted as in (b).

2.7 | NMD Impairment Reduces Virus Accumulation in the Early Infection Stage

For RNA viruses, the timing of viral gene expression is crucial. Specifically, viral proteins that are not essential for replication, such as MP and CP, are typically synthesised later than the viral replicase proteins. This timing prevents these proteins from competing with replicase for viral RNA templates during the early stages of infection, thereby promoting successful viral infection. In the case of CMV, MP is synthesised directly from RNA3 and is produced concurrently with replicase proteins 1a and 2a. This raises the question of whether simultaneous MP production impacts CMV replication efficiency during the early stages of infection. To explore this, we assessed the effect of *trans*-expressed CMV MP on the replication of CMV RNA1 and RNA2 in the absence of RNA3 via agroinfiltration assays. At 2 DPAI, RNA gel blot analysis showed that MP expression reduced replication levels of RNA1 and RNA2 by approximately 40% compared to the vector control (V) or GFP expression (Figure 7a). This suggests that during early infection, overproduction of MP may compromise CMV replication by competing with the replicase for viral RNAs.

Inspired by this finding, we hypothesised that NMD might facilitate CMV replication by degrading RNA3 during the early stages of infection. To test this, we conducted agroinfiltration assays in *N. benthamiana* plants coexpressing CMV RNAs with either UPF1 or U1D. Viral RNAs were detected in infiltrated leaves at 12-h intervals using northern blot hybridisation (Figure 7b). At 12 h postagroinfiltration (HPAI), viral RNAs were undetectable in leaves coexpressing either UPF1 or U1D. By 24 HPAI, RNA1, RNA2 and RNA3 were detected in the UPF1-treated samples, but not in the U1D-treated samples. After another 12 h, both UPF1- and U1D-treated samples showed similarly high levels of viral RNAs. These findings suggest that NMD favours CMV

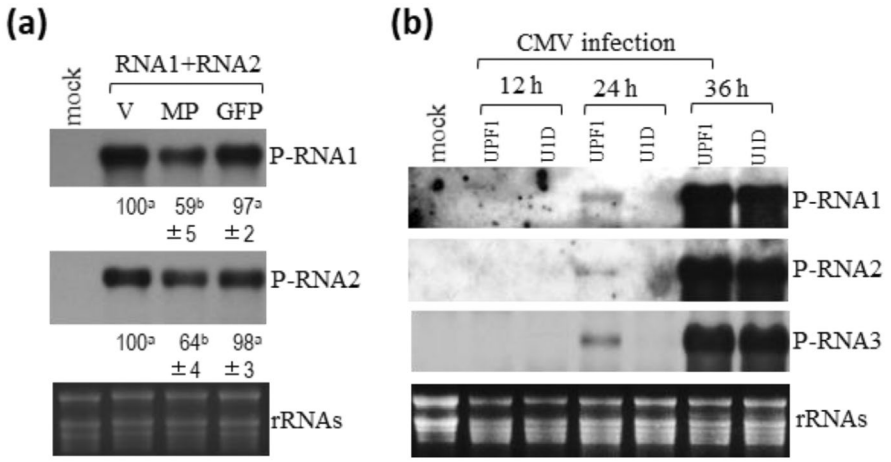

FIGURE 7 | Nonsense-mediated mRNA decay (NMD) contributes to the early stages of viral infection in plants. (a) *Trans*-expression of movement protein (MP) inhibits the replication of viral RNAs. CMV RNA1 and RNA2 were coexpressed with a control vector (pBI121), MP or GFP in *Nicotiana benthamiana* leaves via agroinfiltration. At 3 days postagroinfiltration, infiltrated leaves were collected for RNA extraction, followed by northern blot analysis of the accumulation of RNA1 and RNA2. The relative accumulation levels of the viral RNAs were calculated from three independent biological experiments with standard errors. Paired *t* test was used to analyse statistical significance. Different superscript letters indicate statistical difference at $p < 0.05$. (b) Effect of NMD impairment on virus infection in plants. *Agrobacterium* cells carrying CMV infectious clones were coinfiltrated with bacterial cells expressing either UPF1 or U1D into the sixth true leaves of *N. benthamiana*. Viral RNAs 1–3 were detected separately in the infiltrated leaves using RNA-specific probes at 12, 24 and 36 h postagroinfiltration. P-RNA1, P-RNA2 and P-RNA3 refer to 5′-digoxin labelled probes specific to RNA1, RNA2 and RNA3, respectively.

infection during the early stages of infection, most probably by reducing the MP synthesis.

3 | Discussion

In this study, we investigated the molecular interplay between CMV and NMD. Our data demonstrate that CMV RNA3, but not RNA1 or RNA2, is a target of NMD, which is triggered by the CP nucleotide sequence. The IGR sequence, located immediately downstream of the RNA3 translation termination, does not induce NMD. This is regulated by the nucleotide sequences at its 5′ and 3′ ends. CMV 1a and CP can enhance RNA3 stability as evidenced by the increased accumulation, which is probably due to these viral proteins shielding RNA3 from entering translation, thereby avoiding NMD antiviral defence. Importantly, we found that NMD facilitates CMV accumulation during the early stages of infection. This facilitation might occur due to NMD-mediated RNA3 degradation, as the MP protein, the translation product of RNA3, negatively regulates viral RNA replication.

In nature, the quantity of viral particles transmitted through mechanical means or insect vectors is typically limited (Whitfield et al. 2015; McCrone and Lauring 2018). For (+) RNA viruses, the initial step of infection involves the release of viral RNA genomes from viral particles in host cells, followed by their translation into viral proteins essential for replication. Therefore, to successfully establish an infection, it is crucial for (+) RNA viruses to evade NMD during the translation process. Our findings suggest that genomic segmentation of CMV ensures its replicase-encoding RNAs efficiently evade NMD. While genomic segmentation is rarely featured in (+) RNA viruses infecting animals and humans, it is prevalent in plant RNA viruses. Approximately 10 families of plant viruses have genomes composed of two or more segmented RNAs (Walker et al. 2021). In addition to CMV, well-known segmented (+) RNA viruses include scientifically and economically significant viruses such as BMV, tobacco rattle virus and broad bean wilt virus 2 (Scholthof et al. 2011; Liu et al. 2019). Furthermore, some viruses that cause severe crop damage, such as rice black stripe dwarf virus and rice dwarf virus, possess genomes composed of over 10 double-stranded RNAs (Wu et al. 2024). In segmented RNA viruses, RdRP is typically encoded by a monocistronic RNA, which is probably resistant to NMD due to the absence of a long 3′ UTR. Thus, we speculate that genomic segmentation is one of the general strategies employed by a number of segmented RNA viruses to avoid NMD. This approach is conceptually similar to the strategy employed by potyviruses, which encode a single large ORF in their nonsegmented genomes (Garcia et al. 2014).

Undoubtedly, NMD serves as a universal antiviral defence mechanism, playing an important role in inhibiting viral infections. Interestingly, our data suggest that NMD can promote the initial infection of CMV. We believe this seemingly paradoxical role of NMD arises from differences in its targets. In previous studies, the viral RNA degraded by NMD typically is the viral genome used to produce viral replicase (Balistreri et al. 2014; Garcia et al. 2014; Fontaine et al. 2018; May et al. 2018; Wada et al. 2018; Li et al. 2019; Chen et al. 2024). This degradation reduces the synthesis of viral replicase, thereby diminishing viral RNA replication. In contrast, for CMV, the target of NMD-mediated degradation is RNA3, which serves as a template for the production of MP (Figure 2). Typically, viral MP is produced from subgenomic RNAs, which are synthesised later than the replication-associated proteins, aligning with the temporal sequence of viral infection. However, CMV MP is produced concurrently with the replication components. Notably, CMV MP binds not only to viral RNAs (Li and Palukaitis 1996; Vaquero et al. 1997) but also to the 2a protein (Hwang et al. 2005). Overexpression of the MP could

lead to competition with CMV 1a protein for viral RNAs and the 2a protein, thereby impairing the assembly of the viral replication complex and subsequent replication. This hypothesis is supported by the experimental data showing that *trans*-expression of CMV MP significantly reduced viral RNA replication (Figure 7a). Consequently, we propose a model where NMD facilitates the early infection of CMV. During the initial stages of CMV infection, NMD-resistant RNA1 and RNA2 are efficiently translated to produce viral replicases 1a and 2a. Simultaneously, the virus exploits NMD to selectively target RNA3, accelerating its turnover. This targeted degradation would reduce MP synthesis, as RNA3 serves as the mRNA template for MP production, thereby alleviating competition between the MP and 1a proteins. This, in turn, benefits the 1a protein in recruiting the 2a protein and viral RNAs, leading to enhanced multiplication of viral RNAs in the initial infection cells (Figure 8).

Our work demonstrates that NMD-targeted degradation of RNA3 and its variants depends on the CP nucleotide sequence, rather than the IGR and 3′ UTR. Moreover, both 5′ and 3′ halves of the CP sequence are engaged in the activation of NMD (Figure 3). This indicates that NMD induction requires specific RNA features. Imamachi and colleagues reported that phosphorylated UPF1 prefers to bind GC-rich stretches in the 3′ UTR, which are associated with accelerated RNA decay (Imamachi et al. 2017). We found that both 5′ and 3′ halves of the CP sequence have a local region with an unusually high GC content (Figure 4). Therefore, we speculate that these GC-rich regions could be responsible for the CP sequence inducing NMD.

Our results demonstrate that the IGR sequence is not engaged in NMD activation, which could be the presence of the AU-rich feature at both 5′ and 3′ ends (Figure 4). In the absence of viral proteins, the IGR sequence is not effective in alleviating the CP sequence-triggered decay of RNA3 or its reporter. Even NMD-resistant TCV 3′ UTR in the context of the IGR cannot inhibit CP-induced RNA decay either (Figure S2). Interestingly, we found that CMV 1a replicase provided in trans helps the reporter R3gfp escape from RNA decay by specific interaction with the Box-B motif in the IGR (Figure 6). This is consistent with previous findings that BMV 1a protein stabilises viral RNA3 by recruiting it into viral replication compartments via the 1a–Box-B interaction (Sullivan and Ahlquist 1999; Liu et al. 2009). Such specific interactions between an RNA-binding protein and its target sequence that confer NMD resistance are not common. For instance, host PTBP1 and viral MP proteins can confer NMD resistance, but they often have very poor sequence specificity (Ge et al. 2016; May et al. 2020). As for (+) RNA viruses, viral genomes must be recruited by viral replicase for replication; thus, specific interaction between viral replicase and genomic RNAs would be a generic strategy to avoid viral RNA decay.

In conclusion, this study explored the molecular interaction between NMD and CMV, revealing that CMV RNA3, unlike RNA1 and RNA2, is specifically targeted by NMD, a process triggered by the CP sequence. This targeting by NMD is proposed to facilitate CMV replication during the early stages of infection. Therefore, we propose that genomic segmentation is one of the viral strategies that help segmented RNA viruses evade NMD, highlighting its significant implication in NMD–virus interactions.

4 | Experimental Procedures

4.1 | Plant Growth

Nicotiana benthamiana plants were grown in a plant growth room under a 16-h light period at an intensity of 150–200 μmol m^{-2}s^{-1} and a temperature of 23°C–25°C. Seedlings

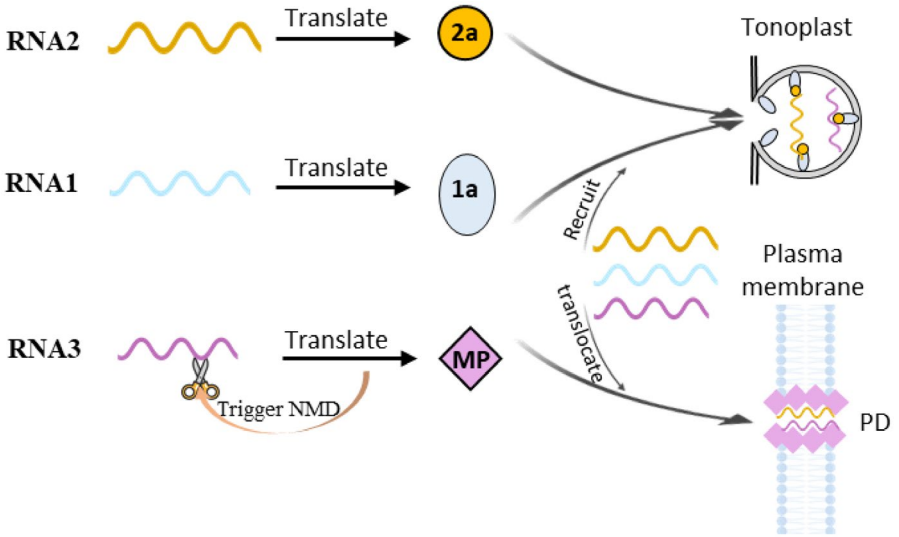

FIGURE 8 | Proposed model of how nonsense-mediated mRNA decay (NMD) facilitates early CMV infection. During the initial stages of CMV infection, NMD-resistant RNA1 and RNA2 are efficiently translated to produce viral replicases 1a and 2a. Concurrently, the virus exploits the NMD pathway to selectively target RNA3 for accelerated degradation. This degradation would reduce the synthesis of the movement protein (MP), thereby alleviating competition for viral RNAs and their translocation to plasmodesmata (PD). This, in turn, facilitates the 1a protein to recruit the 2a protein and viral RNAs, enhancing viral RNA replication in the initial infection cells.

approximately 4 weeks old were used for agroinfiltration experiments.

4.2 | Plasmid Construction

The T-DNA-based infectious clones pCB301-C1, pCB301-C2 and pCB301-C3, corresponding to the genomic RNA1, RNA2 and RNA3 of Fny-CMV, respectively, have been previously described (Gao et al. 2018). The DNA constructs pCB301-1a, pCB301-2a and pBI121-Fny2b, used for the transient expression of CMV 1a, 2a and 2b proteins, respectively, were also previously reported (Du et al. 2014; Gao et al. 2018). To transiently express the MP or CP of Fny-CMV in *N. benthamiana*, DNA fragments corresponding to their coding sequences were amplified from pCB301-C3 and inserted into the binary vector pBI121 after digestion with restriction endonucleases BamHI and SacI. For the transient expression of UPF1, the coding sequence for *Arabidopsis* UPF1 (accession: At5g47010) was amplified via reverse transcription (RT)-PCR using specific primers. The resultant PCR product was digested with EcoRI and PstI and inserted into the binary vector pCambia3101, generating pCambia-UPF1. A dominant-negative mutant of UPF1, pCambia-U1D, was generated by substituting the arginine at position 863 with a cysteine, as previously reported (Kertesz et al. 2006). The plasmid pBI121-mCherry was constructed by inserting the coding sequence of mCherry between the BamHI and SacI sites in pBI121. Using the ligation-independent cloning method (Jeong et al. 2012), the 5′ proximal ORFs of CMV genomic RNAs in pCB301-C1, pCB301-C2 and pCB301-C3 were replaced with GFP, generating pCB301-R1gfp, pCB301-R2gfp and pCB301-R3gfp, respectively. Additionally, the sequence spanning from MP to CP in pCB301-C3 was replaced with GFP, creating pCB301-R3gfpΔmp-cp.

Site-directed mutagenesis (Liu and Naismith 2008) was used to introduce specific mutations or delete DNA fragments in the constructs. To prematurely terminate the translation of the 1a protein, codons $_{1100}$TTG or $_{2096}$AAT in RNA1 were changed to the stop codon TAG, generating pCB301-R1$_{PTC1100}$ and pCB301-R1$_{PTC2096}$, respectively. Similarly, codons $_{1095}$CCG or $_{1884}$GAC in RNA2 were replaced with TAG, generating pCB301-R2$_{PTC1095}$ and pCB301-R2$_{PTC1884}$, respectively. To express GFP-fused CP protein, the stop codon of GFP was removed in pCB301-R3gfpΔigr, generating pCB301-R3gfp → cp. To identify the NMD inducer in R3gfp, the IGR, the 5′ half (nt 1–329) or the 3′ half (nt 330–657) of the CP in pCB301-R3gfp was deleted, generating pCB301-R3gfpΔigr, pCB301-R3gfpΔcp$_{1\text{-}329}$ and pCB301-R3gfpΔcp$_{330\text{-}657}$, respectively. The entire CP was also removed, creating pCB301-R3gfpΔcp. Furthermore, the IGR and either the 5′ or 3′ half of the CP were deleted from pCB301-R3gfp, generating pCB301-ΔigrΔcp$_{1\text{-}329}$ and pCB301-ΔigrΔcp$_{330\text{-}657}$, respectively. A 54-nt fragment corresponding to the putative amphipathic helix A (amino acid residues 422–439) in CMV 1a protein was deleted from pCB301-C1a, creating the mutant pCB301-C1aΔ18H. The Box-B motif was removed from pCB301-R3gfp to create the mutant pCB301-R3gfpΔBoxB. The plasmids pCB301-Δseg1, pCB301-Δseg2 and pCB301-Δseg3 were derivatives of pCB301-R3gfpΔcp, created by deleting segments at the 5′ end (nt 1–110), middle (nt 111–212) or 3′ end (nt 213–297) of the IGR, respectively, using site-directed mutagenesis. All constructs were confirmed by sequencing before transformation into *Agrobacterium* cells. The primers used in these plasmid constructions are listed in Table S2.

4.3 | *Agrobacterium* Transformation and Infiltration

All plasmids used in this study were transformed into *Agrobacterium tumefaciens* GV3101 using the freeze–thaw method (Weigel and Glazebrook 2006). Agroinfiltration assays followed the procedure described previously (He et al. 2019). For analyses of RNA accumulation in plants, *Agrobacterium* cells carrying plasmids expressing CMV RNAs or their derivatives were mixed with cells containing pBI121-mCherry and 35:P19. The mixture was infiltrated into the sixth true leaf of *N. benthamiana*. For the transient expression of UPF1, U1D, or viral proteins, *Agrobacterium* cells carrying pCambia-UPF1, pCambia-U1D, or the respective viral protein-expressing plasmids were included in the agroinfiltration. Two DPAI, the infiltrated leaves were subjected to fluorescence visualisation, western blot analysis for GFP and mCherry, or northern blot analysis for RNA as described below. For viral RNA accumulation analysis in the presence of UPF1 or U1D, *Agrobacterium* cells carrying the infectious clones of CMV were co-infiltrated with cells containing pCambia-UPF1 or pCambia-U1D into the sixth true leaves of *N. benthamiana* plants. Infiltrated leaves from three plants were collected at time points from 12 to 48 HPAI in 12 h intervals for RNA extraction and subsequent RNA gel blot analysis.

4.4 | Fluorescence Visualisation

Lower epidermal cells of infiltrated leaves were imaged at 2 DPAI using a Leica SP5 laser confocal microscope to analyse the fluorescence intensities of GFP and mCherry. Optical parameters for visualising both fluorescent proteins, such as laser excitation intensity, were kept constant across all leaf samples within the same batch.

4.5 | Northern Blot Hybridization

RNA gel blot assays followed the procedure described previously (He et al. 2019). Briefly, total RNAs were extracted from infiltrated leaves using extraction buffer (0.05 M sodium acetate pH 5.2, 0.01 M EDTA pH 8.0, 1% SDS), separated in a 1.5% agarose gel containing 7% formaldehyde, and transferred onto a positively charged nylon membrane (GE). RNA transcripts produced from *Agrobacterium*-delivered T-DNAs were detected using a probe mixture composed of three gene-specific DNA oligonucleotides labelled with digoxin (DIG) at the 3′ end, using the DIG oligonucleotide tailing kit (Roche) as per the manufacturer's instructions. GFP-specific probes were used to detect R3gfp and its derivatives. The oligonucleotides used are listed in Table S3.

4.6 | Western Blot Hybridization

GFP and mCherry proteins were detected following the method described previously (Du et al. 2014). In brief, total proteins were extracted from infiltrated leaves using 1× phosphate buffer, denatured in 1× Laemmli buffer (Laemmli 1970) and subjected to SDS-PAGE. Proteins were then transferred onto a nitrocellulose membrane (GE) and incubated with polyclonal antibodies against GFP or mCherry (Santa Cruz), followed by incubation with horseradish peroxidase-conjugated secondary antibodies (AbCam). Detection was carried out using enhanced chemiluminescence solution (Thermo Fisher).

4.7 | Sequence Analysis and RNA Structure Prediction

GC content analyses of the IGR, CP (5′ and 3′ halves) and 3′ UTR from Fny-CMV were conducted using the Editseq program in DNAstar software. In-house Perl scripts were used to scan GC content in a 50-nt window with a step size of one base for the RNA3 3′ NTS sequence, ranging from the IGR to 3′ UTR. RNA structure predictions for the IGR were based on the predicted IGR of Bn57-CMV, which was chemically probed in plant cell lysates (Watters et al. 2018). RNA structures were drawn using RNAdrawer 2.0 (Johnson et al. 2019).

4.8 | Statistical Analysis

Different significance was evaluated by conducting paired *t* test or one-way ANOVA using Microsoft Excel. A *p* value of 0.05 was set as the threshold for significance.

Acknowledgements

We thank Professor Dongliang Yu for providing assistance in scanning the GC content. This research was funded by the National Natural Science Foundation of China (31870144, 32070154 to Z.D.).

Conflicts of Interest

The authors declare no conflicts of interest.

Data Availability Statement

The data that supports the findings of this study are available in the Supporting Information of this article.

References

Ahmed, M. R., and Z. Du. 2023. "Molecular Interaction of Nonsense-Mediated mRNA Decay With Viruses." *Viruses* 15, no. 4: 816. https://doi.org/10.3390/v15040816.

Baker, S. L., and J. R. Hogg. 2017. "A System for Coordinated Analysis of Translational Readthrough and Nonsense-Mediated mRNA Decay." *PLoS One* 12: e0173980.

Balistreri, G., C. Bognanni, and O. Muhlemann. 2017. "Virus Escape and Manipulation of Cellular Nonsense-Mediated mRNA Decay." *Viruses* 9, no. 1: 24. https://doi.org/10.3390/v9010024.

Balistreri, G., P. Horvath, C. Schweingruber, et al. 2014. "The Host Nonsense-Mediated mRNA Decay Pathway Restricts Mammalian RNA Virus Replication." *Cell Host and Microbe* 16: 403–411.

Baumstark, T., and P. Ahlquist. 2001. "The Brome Mosaic Virus RNA3 Intergenic Replication Enhancer Folds to Mimic a tRNA TpsiC-Stem Loop and Is Modified In Vivo." *RNA* 7: 1652–1670.

Canto, T., D. A. Prior, K. H. Hellwald, K. J. Oparka, and P. Palukaitis. 1997. "Characterization of Cucumber Mosaic Virus. IV. Movement Protein and Coat Protein Are Both Essential for Cell-To-Cell Movement of Cucumber Mosaic Virus." *Virology* 237: 237–248.

Chang, Y. F., J. S. Imam, and M. F. Wilkinson. 2007. "The Nonsense-Mediated Decay RNA Surveillance Pathway." *Annual Review of Biochemistry* 76: 51–74.

Chen, Y. L., M. X. Jia, L. H. Ge, et al. 2024. "A Negative Feedback Loop Compromises NMD-Mediated Virus Restriction by the Autophagy Pathway in Plants." *Advanced Science* 11: 2400978.

Cillo, F., I. M. Roberts, and P. Palukaitis. 2002. "In Situ Localization and Tissue Distribution of the Replication-Associated Proteins of Cucumber Mosaic Virus in Tobacco and Cucumber." *Journal of Virology* 76: 10654–10664.

Contu, L., G. Balistreri, M. Domanski, A. C. Uldry, and O. Muhlemann. 2021. "Characterisation of the Semliki Forest Virus–Host Cell Interactome Reveals the Viral Capsid Protein as an Inhibitor of Nonsense-Mediated mRNA Decay." *PLoS Pathogens* 17: e1009603.

den Boon, J. A., and P. Ahlquist. 2010. "Organelle-Like Membrane Compartmentalization of Positive-Strand RNA Virus Replication Factories." *Annual Review of Microbiology* 64: 241–256.

Ding, S. W. 2010. "RNA-Based Antiviral Immunity." *Nature Reviews Immunology* 10: 632–644.

Ding, S. W., B. J. Anderson, H. R. Haase, and R. H. Symons. 1994. "New Overlapping Gene Encoded by the Cucumber Mosaic Virus Genome." *Virology* 198: 593–601.

Ding, S. W., and O. Voinnet. 2014. "Antiviral RNA Silencing in Mammals: No News Is Not Good News." *Cell Reports* 9: 795–797.

Du, K., D. Peng, J. Wu, et al. 2024. "Maize Splicing-Mediated mRNA Surveillance Impeded by Sugarcane Mosaic Virus-Coded Pathogenic Protein NIa-Pro." *Science Advances* 10: eadn3010.

Du, Z., A. Chen, W. Chen, et al. 2014. "Nuclear-Cytoplasmic Partitioning of Cucumber Mosaic Virus Protein 2b Determines the Balance Between Its Roles as a Virulence Determinant and an RNA-Silencing Suppressor." *Journal of Virology* 88: 5228–5241.

Emmott, E., D. Munday, E. Bickerton, et al. 2013. "The Cellular Interactome of the Coronavirus Infectious Bronchitis Virus Nucleocapsid Protein and Functional Implications for Virus Biology." *Journal of Virology* 87: 9486–9500.

Fontaine, K. A., K. E. Leon, M. M. Khalid, et al. 2018. "The Cellular NMD Pathway Restricts Zika Virus Infection and Is Targeted by the Viral Capsid Protein." *mBio* 9, no. 6: e02126-18. https://doi.org/10.1128/mBio.02126-18.

Gao, S., J. Lu, X. Cheng, Z. Gu, Q. Liao, and Z. Du. 2018. "Heterologous Replicase From Cucumoviruses Can Replicate Viral RNAs, but Is Defective in Transcribing Subgenomic RNA4A or Facilitating Viral Movement." *Viruses* 10, no. 11: 590. https://doi.org/10.3390/v10110590.

Garcia, D., S. Garcia, and O. Voinnet. 2014. "Nonsense-Mediated Decay Serves as a General Viral Restriction Mechanism in Plants." *Cell Host and Microbe* 16: 391–402.

Ge, Z., B. L. Quek, K. L. Beemon, and J. R. Hogg. 2016. "Polypyrimidine Tract Binding Protein 1 Protects mRNAs From Recognition by the Nonsense-Mediated mRNA Decay Pathway." *eLife* 5: e11155. https://doi.org/10.7554/eLife.11155.

Gordon, D. E., G. M. Jang, M. Bouhaddou, et al. 2020. "A SARS-CoV-2 Protein Interaction Map Reveals Targets for Drug Repurposing." *Nature* 583: 459–468. https://doi.org/10.1038/s41586-020-2286-9.

He, H., L. Ge, Y. Chen, et al. 2024. "m(6)A Modification of Plant Virus Enables Host Recognition by NMD Factors in Plants." *Science China Life Sciences* 67: 161–174.

He, L., Q. Wang, Z. Gu, Q. Liao, P. Palukaitis, and Z. Du. 2019. "A Conserved RNA Structure Is Essential for a Satellite RNA-Mediated Inhibition of Helper Virus Accumulation." *Nucleic Acids Research* 47: 8255–8271.

Hogg, J. R., and S. P. Goff. 2010. "Upf1 Senses 3′UTR Length to Potentiate mRNA Decay." *Cell* 143: 379–389.

Hwang, M. S., S. H. Kim, J. H. Lee, J. M. Bae, K. H. Paek, and Y. I. Park. 2005. "Evidence for Interaction Between the 2a Polymerase Protein and the 3a Movement Protein of Cucumber Mosaic Virus." *Journal of General Virology* 86: 3171–3177.

Imamachi, N., K. A. Salam, Y. Suzuki, and N. Akimitsu. 2017. "A GC-Rich Sequence Feature in the 3′ UTR Directs UPF1-Dependent mRNA Decay in Mammalian Cells." *Genome Research* 27: 407–418.

Jeong, J. Y., H. S. Yim, J. Y. Ryu, et al. 2012. "One-Step Sequence- and Ligation-Independent Cloning as a Rapid and Versatile Cloning Method for Functional Genomics Studies." *Applied and Environmental Microbiology* 78: 5440–5443.

Johnson, P. Z., W. K. Kasprzak, B. A. Shapiro, and A. E. Simon. 2019. "RNA2Drawer: Geometrically Strict Drawing of Nucleic Acid Structures With Graphical Structure Editing and Highlighting of Complementary Subsequences." *RNA Biology* 16: 1667–1671.

Kalyna, M., C. G. Simpson, N. H. Syed, et al. 2012. "Alternative Splicing and Nonsense-Mediated Decay Modulate Expression of Important Regulatory Genes in Arabidopsis." *Nucleic Acids Research* 40: 2454–2469.

Kashima, I., A. Yamashita, N. Izumi, et al. 2006. "Binding of a Novel SMG-1-Upf1-eRF1-eRF3 Complex (SURF) to the Exon Junction Complex Triggers Upf1 Phosphorylation and Nonsense-Mediated mRNA Decay." *Genes & Development* 20: 355–367. https://doi.org/10.1101/gad.1389006.

Kertesz, S., Z. Kerenyi, Z. Merai, et al. 2006. "Both Introns and Long 3′-UTRs Operate as Cis-Acting Elements to Trigger Nonsense-Mediated Decay in Plants." *Nucleic Acids Research* 34: 6147–6157.

Laemmli, U. K. 1970. "Cleavage of Structural Proteins During the Assembly of the Head of Bacteriophage T4." *Nature* 227: 680–685.

Li, F., and A. Wang. 2018. "RNA Decay Is an Antiviral Defense in Plants That Is Counteracted by Viral RNA Silencing Suppressors." *PLoS Pathogens* 14: e1007228.

Li, F., and A. Wang. 2019. "RNA-Targeted Antiviral Immunity: More Than Just RNA Silencing." *Trends in Microbiology* 27: 792–805.

Li, M., J. R. Johnson, B. Truong, et al. 2019. "Identification of Antiviral Roles for the Exon-Junction Complex and Nonsense-Mediated Decay in Flaviviral Infection." *Nature Microbiology* 4: 985–995.

Li, Q., and P. Palukaitis. 1996. "Comparison of the Nucleic Acid- and NTP-Binding Properties of the Movement Protein of Cucumber Mosaic Cucumovirus and Tobacco Mosaic Tobamovirus." *Virology* 216: 71–79.

Liu, H., and J. H. Naismith. 2008. "An Efficient One-Step Site-Directed Deletion, Insertion, Single and Multiple-Site Plasmid Mutagenesis Protocol." *BMC Biotechnology* 8: 91.

Liu, L., W. M. Westler, J. A. den Boon, et al. 2009. "An Amphipathic Alpha-Helix Controls Multiple Roles of Brome Mosaic Virus Protein 1a in RNA Replication Complex Assembly and Function." *PLoS Pathogens* 5: e1000351.

Liu, Y., F. Li, Y. Li, et al. 2019. "Identification, Distribution and Occurrence of Viruses in the Main Vegetables of China." *Scientia Agricultura Sinica* 52: 239–261.

Lopez-Gomollon, S., and D. C. Baulcombe. 2022. "Roles of RNA Silencing in Viral and Non-Viral Plant Immunity and in the Crosstalk Between Disease Resistance Systems." *Nature Reviews Molecular Cell Biology* 23: 645–662.

May, J. P., P. Z. Johnson, M. Ilyas, F. Gao, and A. E. Simon. 2020. "The Multifunctional Long-Distance Movement Protein of Pea Enation Mosaic Virus 2 Protects Viral and Host Transcripts From Nonsense-Mediated Decay." *mBio* 11: e00204-20. https://doi.org/10.1128/mBio.00204-20.

May, J. P., X. Yuan, E. Sawicki, and A. E. Simon. 2018. "RNA Virus Evasion of Nonsense-Mediated Decay." *PLoS Pathogens* 14: e1007459.

McCrone, J. T., and A. S. Lauring. 2018. "Genetic Bottlenecks in Intraspecies Virus Transmission." *Current Opinion in Virology* 28: 20–25.

Noueiry, A. O., and P. Ahlquist. 2003. "Brome Mosaic Virus RNA Replication: Revealing the Role of the Host in RNA Virus Replication." *Annual Review of Phytopathology* 41: 77–98.

Poch, O., I. Sauvaget, M. Delarue, and N. Tordo. 1989. "Identification of Four Conserved Motifs Among the RNA-Dependent Polymerase Encoding Elements." *EMBO Journal* 8: 3867–3874.

Popp, M. W., H. Cho, and L. E. Maquat. 2020. "Viral Subversion of Nonsense-Mediated mRNA Decay." *RNA* 26: 1509–1518.

Ramage, H. R., G. R. Kumar, E. Verschueren, et al. 2015. "A Combined Proteomics/Genomics Approach Links Hepatitis C Virus Infection With Nonsense-Mediated mRNA Decay." *Molecular Cell* 57: 329–340.

Restrepo-Hartwig, M., and P. Ahlquist. 1999. "Brome Mosaic Virus RNA Replication Proteins 1a and 2a Colocalize and 1a Independently Localizes on the Yeast Endoplasmic Reticulum." *Journal of Virology* 73: 10303–10309.

Sarkar, R., S. Banerjee, A. Mukherjee, and M. Chawla-Sarkar. 2022. "Rotaviral Nonstructural Protein 5 (NSP5) Promotes Proteasomal Degradation of Up-Frameshift Protein 1 (UPF1), a Principal Mediator of Nonsense-Mediated mRNA Decay (NMD) Pathway, to Facilitate Infection." *Cellular Signalling* 89: 110180.

Scholthof, K. B., S. Adkins, H. Czosnek, et al. 2011. "Top 10 Plant Viruses in Molecular Plant Pathology." *Molecular Plant Pathology* 12: 938–954. https://doi.org/10.1111/j.1364-3703.2011.00752.x.

Shoemaker, C. J., and R. Green. 2012. "Translation Drives mRNA Quality Control." *Nature Structural & Molecular Biology* 19: 594–601.

Sullivan, M. L., and P. Ahlquist. 1999. "A Brome Mosaic Virus Intergenic RNA3 Replication Signal Functions With Viral Replication Protein 1a to Dramatically Stabilize RNA In Vivo." *Journal of Virology* 73: 2622–2632.

Tang, X., Y. Zhu, S. L. Baker, et al. 2016. "Structural Basis of Suppression of Host Translation Termination by Moloney Murine Leukemia Virus." *Nature Communications* 7: 12070.

Tran, G. V. Q., J. Kleinehr, H. F. Preugschas, et al. 2021. "Nonsense-Mediated mRNA Decay Does Not Restrict Influenza A Virus Propagation." *Cellular Microbiology* 23: e13323.

Traynor, P., B. M. Young, and P. Ahlquist. 1991. "Deletion Analysis of Brome Mosaic Virus 2a Protein: Effects on RNA Replication and Systemic Spread." *Journal of Virology* 65: 2807–2815.

Vaquero, C., Y. C. Liao, J. Nahring, and R. Fischer. 1997. "Mapping of the RNA-Binding Domain of the Cucumber Mosaic Virus Movement Protein." *Journal of General Virology* 78: 2095–2099.

Wada, M., K. G. Lokugamage, K. Nakagawa, K. Narayanan, and S. Makino. 2018. "Interplay Between Coronavirus, a Cytoplasmic RNA Virus, and Nonsense-Mediated mRNA Decay Pathway." *Proceedings of the National Academy of Sciences of the United States of America* 115: E10157–E10166.

Walker, P. J., S. G. Siddell, E. J. Lefkowitz, et al. 2021. "Changes to Virus Taxonomy and to the International Code of Virus Classification and

Nomenclature Ratified by the International Committee on Taxonomy of Viruses (2021)." *Archives of Virology* 166: 2633–2648.

Watters, K. E., K. Choudhary, S. Aviran, J. B. Lucks, K. L. Perry, and J. R. Thompson. 2018. "Probing of RNA Structures in a Positive Sense RNA Virus Reveals Selection Pressures for Structural Elements." *Nucleic Acids Research* 46: 2573–2584.

Weigel, D., and J. Glazebrook. 2006. "Transformation of *Agrobacterium* Using the Freeze-Thaw Method." *CSH Protocols* 2006: pdb.prot4666.

Whitfield, A. E., B. W. Falk, and D. Rotenberg. 2015. "Insect Vector-Mediated Transmission of Plant Viruses." *Virology* 479–480: 278–289.

Withers, J. B., and K. L. Beemon. 2011. "The Structure and Function of the Rous Sarcoma Virus RNA Stability Element." *Journal of Cellular Biochemistry* 112: 3085–3092.

Wu, J., Y. Zhang, F. Li, et al. 2024. "Plant Virology in the 21st Century in China: Recent Advances and Future Directions." *Journal of Integrative Plant Biology* 66: 579–622.

Xin, H. W., L. H. Ji, S. W. Scott, R. H. Symons, and S. W. Ding. 1998. "Ilarviruses Encode a Cucumovirus-Like 2b Gene That Is Absent in Other Genera Within the *Bromoviridae*." *Journal of Virology* 72: 6956–6959.

Supporting Information

Additional supporting information can be found online in the Supporting Information section.